




# Plasma Membrane Anchoring and Gag:Gag Multimerization on Viral RNA Are Critical Properties of HIV-1 Gag Required To Mediate Efficient Genome Packaging

Alice Duchon,<sup>a</sup> Steven Santos,<sup>a</sup> Jianbo Chen,<sup>a</sup> Matthew Brown,<sup>a</sup> Olga A. Nikolaitchik,<sup>a</sup> Sheldon Tai,<sup>a</sup> Jeffrey A. Chao,<sup>b</sup> Eric O. Freed,<sup>c</sup> Vinay K. Pathak,<sup>d</sup>  Wei-Shau Hu<sup>a</sup>

<sup>a</sup>Viral Recombination Section, HIV Dynamics and Replication Program, National Cancer Institute, Frederick, Maryland, USA

<sup>b</sup>Friedrich Miescher Institute for Biomedical Research, Basel, Switzerland

<sup>c</sup>Virus-Cell Interaction Section, National Cancer Institute, Frederick, Maryland, USA

<sup>d</sup>Viral Mutation Section, HIV Dynamics and Replication Program, National Cancer Institute, Frederick, Maryland, USA

**ABSTRACT** Human immunodeficiency virus type 1 (HIV-1) Gag selects and packages the HIV RNA genome during virus assembly. However, HIV-1 RNA constitutes only a small fraction of the cellular RNA. Although Gag exhibits a slight preference to viral RNA, most of the cytoplasmic Gag proteins are associated with cellular RNAs. Thus, it is not understood how HIV-1 achieves highly efficient genome packaging. We hypothesize that besides RNA binding, other properties of Gag are important for genome packaging. Many Gag mutants have assembly defects that preclude analysis of their effects on genome packaging. To bypass this challenge, we established complementation systems that separate the particle-assembling and RNA-binding functions of Gag: we used a set of Gag proteins to drive particle assembly and an RNA-binding Gag to package HIV-1 RNA. We have developed two types of RNA-binding Gag in which packaging is mediated by the authentic nucleocapsid (NC) domain or by a nonviral RNA-binding domain. We found that in both cases, mutations that affect the multimerization or plasma membrane anchoring properties of Gag reduce or abolish RNA packaging. These mutant Gag can coassemble into particles but cannot package the RNA genome efficiently. Our findings indicate that HIV-1 RNA packaging occurs at the plasma membrane and RNA-binding Gag needs to multimerize on RNA to encapsidate the viral genome.

**IMPORTANCE** To generate infectious virions, HIV-1 must package its full-length RNA as the genome during particle assembly. HIV-1 Gag:RNA interactions mediate genome packaging, but the mechanism remains unclear. Only a minor portion of the cellular RNA is HIV-1 RNA, and most of the RNAs associated with cytoplasmic Gag are cellular RNAs. However, >94% of the HIV-1 virions contain viral RNA genome. We posited that, besides RNA binding, other properties of Gag contribute to genome packaging. Using two complementation systems, we examined features of Gag that are important for genome packaging. We found that the capacities for Gag to multimerize and to anchor at the plasma membrane are critical for genome packaging. Our results revealed that Gag needs to multimerize on viral RNA at the plasma membrane in order to package RNA genome.

**KEYWORDS** Gag, Gag:RNA interactions, RNA, genome packaging, human immunodeficiency virus, membrane targeting, multimerization

Human immunodeficiency virus type 1 (HIV-1) assembly is a complex process largely orchestrated by the viral Gag polyprotein (1). During assembly, Gag coordinates interactions with viral components to generate particles that contain all elements

**Editor** Stephen P. Goff, Columbia University/HHMI

This is a work of the U.S. Government and is not subject to copyright protection in the United States. Foreign copyrights may apply.

Address correspondence to Wei-Shau Hu, Wei-Shau.Hu@nih.gov.

This article is a direct contribution from Wei-Shau Hu, a Fellow of the American Academy of Microbiology, who arranged for and secured reviews by Akira Ono, University of Michigan Medical School, and Nathan Sherer, University of Wisconsin-Madison.

**Received** 28 October 2021

**Accepted** 1 November 2021

**Published** 7 December 2021

required for successful infection. One essential step is to select and package into virions two copies of the unspliced HIV-1 RNA (referred to as HIV-1 RNA hereafter) from a large pool of cellular RNA (1–4). HIV Gag is composed of matrix (MA), capsid (CA), nucleocapsid (NC), flanked by two short spacer peptides (SP1 and SP2), and p6 domains (1). Discrete functions are carried out by each domain during the virus replication cycle. MA contains a myristylation moiety on the G1 residue, along with a basic residue patch that allows for anchoring of Gag to the plasma membrane. Motifs located within CA are necessary for Gag oligomerization during particle assembly and formation of the capsid core during maturation. NC is comprised of two zinc knuckles that are essential for nucleic acid-binding and chaperone activities. Finally, p6 interacts with host proteins required for viral particle release from the cell (1). However, Gag domains can act cooperatively, and even subtle changes in one domain often impact functions of another. For instance, a disordered region spanning the junction between the CA domain of Gag and SP1 forms a six-helix bundle when bound to inositol hexakisphosphate, assisting in both immature Gag lattice assembly and subsequent capsid maturation (5–7). In addition to genome packaging, the NC domain also plays a role in HIV-1 particle assembly. Deletion of the NC domain leads to assembly defects (8, 9); however, the function of the NC domain in assembly can be replaced by a leucine zipper motif (LZ) (8). The resulting Gag, referred to as GagLZ, can efficiently form morphologically normal immature particles but lacks detectable RNA, including viral RNA (8, 10).

Genome packaging is a highly efficient process in HIV-1 assembly because nearly all particles contain HIV-1 RNA (11). However, the mechanism by which Gag achieves such a high degree of RNA enrichment in virus particles is not well understood. Initially, it was thought that the packaging signal residing in the 5' untranslated region (5' UTR) contained discrete, high-affinity NC binding sites that would allow selection of HIV-1 RNA (12). However, several *in vitro* studies showed that, under physiological conditions, Gag binds cellular and viral RNA in an indistinguishable manner (13–15). In all cases, HIV-1 Gag displays high-affinity binding to any RNA, with an equilibrium dissociation constant ( $K_D$ ) of 25 to 50 nM (13). This has been recapitulated in a cell-based cross-linking-immunoprecipitation (CLIP) sequencing study, which showed that although Gag binds viral RNA with a slight preference (ca. four- to fivefold) relative to cellular RNA, most of the HIV-1 cytoplasmic Gag is associated with cellular RNAs (16). Thus, the high selectivity of RNA packaging cannot be explained solely by the RNA-binding preference of Gag. Therefore, the mechanism by which HIV-1 Gag efficiently packages RNA genome is currently unknown.

We sought to define the mechanisms by which HIV-1 efficiently package its RNA genome. We hypothesized that, in addition to RNA binding, other properties of Gag play essential roles in genome packaging. However, many mutations in Gag cause particle assembly defects, making it difficult to study their genome packaging capabilities. To bypass this issue, we developed complementation systems that separate two essential functions of Gag required in generating infectious viruses: particle assembly and genome packaging. These systems use three Gag constructs, two of which do not bind RNA but can assemble into particles and a third Gag that is capable of binding RNA. This strategy allowed us to study the HIV-1 RNA packaging capabilities of Gag mutants that typically display severe assembly defects. GagLZ can assemble into particles that lack RNA (8, 10); for the particle-assembling Gag, we used GagLZ and a Gag-LZ tagged with cerulean fluorescent protein (CFP). For RNA-binding Gag, we used two different approaches. First, we developed a novel NC-independent packaging system by fusing to Gag an RNA-binding domain from a bacterial protein, BglG (17), that recognizes specific stem-loop sequences inserted into the viral genome. The addition of BglG allowed the modified GagLZ to bind and package HIV-1 RNA independently of NC:RNA interactions. Additionally, we used an NC-based RNA-binding Gag to confirm findings obtained with the nonviral-protein-mediated genome packaging.

To examine genome packaging, we used a fluorescence microscopy-based single virion analysis technique that visualizes viral RNA in individual particles (11).

Coexpression of unmodified Gag and fluorescent-protein-tagged Gag at a 1:1 ratio generates morphologically normal immature particles (18). HIV-1 RNA that is engineered to contain stem-loop sequences can be labeled by RNA-binding proteins tagged with a fluorescent protein. Thus, by labeling Gag and RNA with different fluorescent proteins, individual viral particles can be visualized, and whether they contain viral RNA can be determined using fluorescence microscopy. In this study, we adopted the single virion analysis approach to examine RNA packaging in our complementation system. We have also introduced mutations into the RNA-binding Gag and determined whether such mutations affected RNA packaging. By using this strategy, we were able to demonstrate that mutations in Gag that disrupted plasma membrane binding or Gag:Gag multimerization also caused severe RNA packaging defects. Inhibiting myristylation of Gag was especially detrimental to RNA packaging and could not be rescued by increasing Gag expression. Removal of the C-terminal domain (CTD) of CA or introduction of point mutations that reduce the ability of Gag to oligomerize also diminished RNA packaging efficiency. These results were recapitulated in the context of an NC-dependent packaging system, indicating these features of Gag are necessary in wild-type Gag assembly to facilitate RNA packaging. Taken together, our study demonstrated that in addition to RNA binding, other aspects of HIV-1 Gag, such as membrane targeting and Gag multimerization, are essential for highly efficient HIV-1 RNA packaging. RNA-binding Gag must be anchored to the plasma membrane and be able to multimerize to effectively package HIV-1 RNA. These findings reveal important new insights into an essential step of HIV-1 replication.

## RESULTS

### **HIV-1 genome packaging can be mediated by nonviral RNA-binding protein.**

Many Gag mutants have assembly defects, making it difficult to study their abilities to package the viral genome. To better understand the properties of Gag required for genome packaging, we established a complementation assay that separates two functions of Gag: particle assembly and genome packaging. For the complementation assay, we used three constructs that expressed GagLZ, GagLZ-CFP, and GagLZ-Bgl, in which the NC domain was replaced by a LZ motif (Fig. 1A). GagLZ and GagLZ-CFP, which is GagLZ tagged with cerulean fluorescent protein (CFP), do not package RNA but generate particles, whereas GagLZ-Bgl has an RNA-binding domain. GagLZ-Bgl was constructed by fusing the N-terminal portion of the bacterial RNA-binding protein, BglG, to the C terminus of GagLZ. Each Gag protein was expressed from a nearly full-length HIV construct containing two sets of stem loops, BSL and PSL, located in the *pol* region (Fig. 1A). BglG specifically recognizes the BSL sequences (17), whereas bacteriophage PP7 coat protein specifically binds to PSL sequences (19).

In this system, coassembly of GagLZ and GagLZ-CFP generates CFP-positive (CFP<sup>+</sup>) particles. If GagLZ-Bgl is coassembled into the particle, viral RNA can be packaged via BglG:BSL interactions. Because the viral RNA contains PSL, packaged RNA can be detected by the yellow fluorescent protein (YFP) signal through interactions between PSL and PP7 coat proteins fused to yellow fluorescent protein (PP7-YFP). Therefore, by comparing the proportion of CFP<sup>+</sup> particles that are also YFP<sup>+</sup>, we can determine whether GagLZ-Bgl is capable of packaging viral RNA into particles and the efficiency of such a strategy. To test this system, GagLZ and PP7-YFP expression constructs were cotransfected into 293T cells, supernatants were harvested, clarified by filtration, and plated on slides, and particles were imaged using fluorescence microscopy (single virion analyses). We observed significant numbers of YFP<sup>+</sup> CFP<sup>+</sup> particles among CFP<sup>+</sup> particles in samples that coexpressed GagLZ-Bgl, but not in samples that expressed only GagLZ and GagLZ-CFP (Fig. 1B). These results suggest the possibility that nonviral RNA-binding domain can package RNA genome.

To more quantitatively examine the efficiency of genome packaging by the nonviral RNA-binding domain fused to GagLZ, we performed titration experiments. We cotransfected 293T cells with constant amounts of GagLZ and PP7-YFP expression plasmids

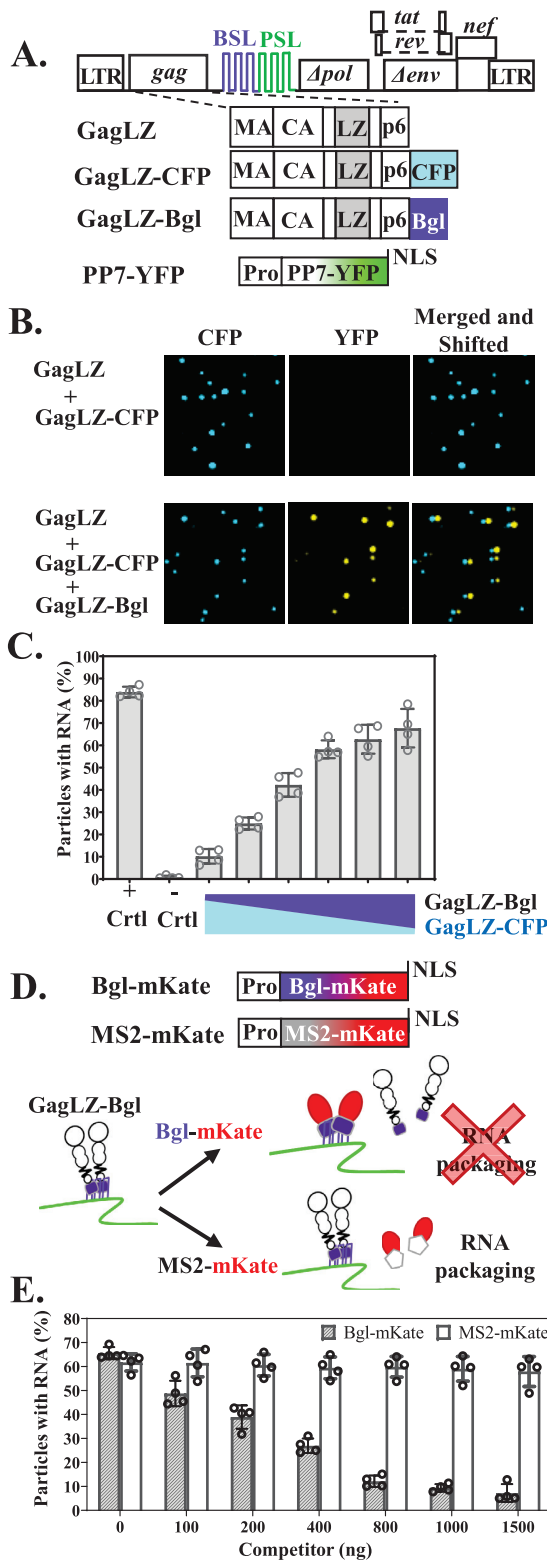


**FIG 1** NC-independent packaging system and experimental approach. (A) General structures of constructs used to express GagLZ, GagLZ-CFP, GagLZ-Bgl, and PP7-YFP. A nuclear localization signal (NLS) is fused to the C terminus of YFP. All constructs contain a leucine zipper motif (LZ; shown in gray) in place of NC and two sets of stem-loop sequences, BSL (purple) and PSL (green), inserted into *pol*, which are recognized by BglG protein and PP7 coat protein, respectively. CFP is shown in blue, BglG in purple, and YFP in green. LTR, long terminal repeat. (B) Representative images of particles generated by GagLZ and GagLZ-CFP (top) and by GagLZ, GagLZ-CFP, and GagLZ-Bgl (bottom). Images from CFP and YFP channels are shown individually or merged and shifted by 4 pixels to visualize colocalized signals. (C) Proportions of RNA

(Continued on next page)

and various amounts of GagLZ-Bgl and GagLZ-CFP constructs. In all samples, half of the GagLZ-expressing plasmid encoded GagLZ, whereas the other half of the GagLZ-expressing plasmids encoded GagLZ-Bgl and GagLZ-CFP. For a positive control, we used two constructs encoding unmodified HIV-1 Gag and Gag-CFP that are expected to form particles containing viral RNAs. For a negative control, we used constructs encoding GagLZ and GagLZ-CFP that generate particles without RNA. RNA packaging efficiencies were defined as the percentage of CFP<sup>+</sup> particles that contained RNA (YFP<sup>+</sup>). In the positive control with unmodified Gag, RNA packaging was efficient, as over 84% of the CFP<sup>+</sup> particles contained viral RNA (YFP<sup>+</sup>) (Fig. 1C). As expected, the negative control with GagLZ and GagLZ-CFP alone produced particles with virtually no viral RNA signals (0.8%). Titration of GagLZ-Bgl into the system, comprising 2.5% to 40% of the total GagLZ transfected, resulted in an increase in particles containing RNA signals (from 10% to 68%).

To ensure that RNA packaging occurred through BglG:BSL interactions, we carried out competition experiments. If RNA packaging is mediated by specific interactions between BSL and the BglG domain in GagLZ-Bgl, then adding free BglG protein not fused to Gag should compete with and disrupt these interactions, leading to a loss of RNA packaging. On the other hand, addition of an unrelated RNA-binding protein into the system, such as the coat protein from bacteriophage MS2, should not affect BglG:BSL interactions and genome packaging (Fig. 1D). For these experiments, we transfected cells with constant amounts of GagLZ, GagLZ-CFP, GagLZ-Bgl, and PP7-YFP plasmids along with gradually increasing amounts of plasmids encoding competitive (Bgl-mKate) or noncompetitive (MS2-mKate) fusion proteins. mKate is a red fluorescent protein (20). The MS2 coat protein specifically recognizes and binds to distinct stem-loop sequences, termed MSL (11). Because the system does not contain MSL sequences, introduction of MS2-mKate did not have an appreciable impact on RNA packaging efficiency (Fig. 1E, white bars). However, we observed that Bgl-mKate competes with GagLZ-Bgl for BSL binding, thereby displacing GagLZ-Bgl and resulting in reduced RNA packaging in a concentration-dependent manner (Fig. 1E, filled bars). These results demonstrate that GagLZ-Bgl specifically packages BSL-harboring RNA through BglG:BSL interactions. Thus, nonviral RNA-binding proteins can be used to replace NC to package RNA into viral particles.

**The intensity of MCH signals in viral particles correlates with the amount of RNA-binding Gag protein.** To define properties of Gag important for genome packaging, we mutated the RNA-binding GagLZ-Bgl and determined the abilities of mutant proteins to bring viral RNA into particles. However, such mutations could result in the loss of coassembly of RNA-binding GagLZ into the particles, complicating the analyses. To ensure that any loss in RNA packaging by mutant RNA-binding GagLZ-Bgl was not simply a consequence of reduced coassembly of GagLZ-Bgl into the particles, we fluo-

#### FIG 1 Legend (Continued)

packaging when different amounts of RNA-binding Gag were used. The sample labeled Gag is the positive control generated from transfection with wild-type Gag and Gag-CFP. With the titration, GagLZ plasmid was maintained at half, whereas plasmids encoding GagLZ-CFP and GagLZ-Bgl together constitute the remaining half of the Gag-encoding plasmid. PP7-YFP was cotransfected in all samples. Proportions of particles with RNA are shown for each condition. The ratios of Gag/Gag-CFP in the positive control (+ Ctrl), GagLZ/GagLZ-CFP in the negative control (- Ctrl), and GagLZ/(GagLZ-CFP + GagLZ-Bgl) of the titration experiments were 1:1. In the titrations, the percentages of transfected GagLZ-Bgl plasmid among the Gag-coding plasmids were 2.5, 5, 10, 20, 25, and 40%. (D) Schematics of Bgl-mKate and MS2-mKate, both containing a C-terminal NLS. Diagram depicting competitive (Bgl-mKate) versus noncompetitive (MS2-mKate) RNA-binding proteins and their impact on genome packaging. Bgl-mKate competes with GagLZ-Bgl for binding to BSL that is present in the viral RNA, resulting in a loss of packaged RNA (top). MS2-mKate cannot recognize BSL present in the viral RNA and should not impact RNA packaging through GagLZ-Bgl:BSL interactions (bottom). (E) A mixture of GagLZ/GagLZ-CFP/GagLZ-Bgl at a 2:1:1 ratio along with PP7-YFP was transfected into cells with increasing amounts of competing (Bgl-mKate) or noncompeting (MS2-mKate), 0 to 1,500 ng. This corresponds to a molar ratio ranging from 1:1 (100 ng) to 1:14 (1,500 ng) GagLZ-Bgl:Bgl-mKate competitor. The percentages of particles containing RNA are depicted for each Bgl-mKate (gray bars) and MS2-YFP (white bars) condition. Results of four independent experiments (open circles) are indicated as means  $\pm$  standard deviations (error bars).

recently tagged GagLZ-Bgl. For this purpose, we inserted an internal mCherry (MCH) fluorescent protein (iC) between the MA and CA domains to generate Gag-iCLZ-Bgl (Fig. 2A). It was previously shown that a fluorescent protein can be inserted into this position in Gag without affecting its ability to coassemble with wild-type Gag (21, 22). Using the MCH signal, we can determine whether Gag-iCLZ-Bgl is coassembled into particles and ensure that any reduction in RNA packaging is not caused by an inability of GagLZ to coassemble into particles. To verify that insertion of iC was not disruptive to RNA packaging, we performed titration experiments with Gag-iCLZ-Bgl similar to those described in the legend to Fig. 1C. We cotransfected cells with GagLZ, GagLZ-CFP, Gag-iCLZ-Bgl, and PP7-YFP expression vectors, harvested particles, and performed single virion analysis. RNA packaging efficiency was determined as a percentage of CFP<sup>+</sup> particles that contained RNA and Gag-iCLZ-Bgl (CFP<sup>+</sup> MCH<sup>+</sup> YFP<sup>+</sup>), whereas coassembly was calculated as the percentage of total GagLZ-containing particles (CFP<sup>+</sup> or MCH<sup>+</sup>) that contained both CFP signal and MCH signal (CFP<sup>+</sup> MCH<sup>+</sup>) (Fig. 2B and C, respectively). In these experiments, the amount of GagLZ plasmid was maintained at the same level, whereas the increased amounts of Gag-iCLZ-Bgl were compensated by decreased amounts of GagLZ-CFP to maintain the same amount of total transfected plasmids. In a similar manner to the GagLZ-Bgl titration results, as the proportion of Gag-iCLZ-Bgl increased in the system, viral RNA packaging also increased (Fig. 2B). Additionally, Gag-iCLZ-Bgl efficiently coassembled with GagLZ-CFP, as a majority of particles contained both CFP and MCH signals (Fig. 2C). In addition, we analyzed more than 2,500 coassembled particles in each sample to determine the median MCH signal intensity in particles. Importantly, an increase in transfected plasmid encoding Gag-iCLZ-Bgl corresponded to an increase in median MCH signal intensity in particles (Fig. 2D). The incorporation of Gag-iCLZ-Bgl was also verified by Western blot analysis of viral lysates (Fig. 2E). Gag-iCLZ-Bgl bands were quantified by densitometry and displayed as a percentage of total Gag species present in viral lysates (Fig. 2E, bottom). To compare results from the two methods used to determine Gag-iCLZ-Bgl incorporation, we plotted the measurements determined by Western blot analyses (y axis) and by the MCH particle intensity (x axis) for each sample (Fig. 2F). We found these two methods showed similar results (Pearson correlation coefficient, 0.91). Together, these findings indicated that insertion of the iC tag did not negatively impact the ability of GagLZ-Bgl to package HIV RNA or coassemble to form particles. Additionally, the MCH signal intensity in particles corresponds to the amounts of Gag-iCLZ-Bgl protein in the particles measured by Western blot analyses and can be used to measure the amount of RNA-binding Gag incorporation.

**Gag membrane localization and multimerization are necessary for NC-independent RNA packaging.** To characterize the properties of Gag required for RNA packaging, we generated a series of truncation mutants by deleting regions of Gag-iCLZ-Bgl from the C terminus of Gag while maintaining Bgl and iC in each protein (Fig. 3A). To examine the ability of each mutant Gag to coassemble and package RNA, GagLZ, GagLZ-CFP, and PP7-YFP were cotransfected alone or with each Gag-iCLZ-Bgl mutant. The efficiencies of coassembly and RNA packaging were calculated as described above. Compared with the packaging efficiencies of the parent Gag-iCLZ-Bgl, deletion of p6 caused little effect, whereas deletion of LZ-p6 resulted in a twofold decrease in packaging efficiencies (Fig. 3B). However, larger deletions extending into SP1 ( $\Delta$ SP1-p6) and CA ( $\Delta$ CTD-p6 and MAiC) exhibited severe packaging defects with efficiencies 11-, 87-, and 108-fold lower than that of unmodified Gag-iCLZ-Bgl, respectively. CA plays a critical role in Gag multimerization. SP1 and a portion of the C terminus of CA (C-terminal domain [CTD]) are known to form a six-helix bundle important for Gag multimerization and particle assembly (5, 6). Thus, these results suggest that multimerization may be an important feature for genome packaging. To investigate whether Gag multimerization affects RNA packaging, we generated two deletion mutants,  $\Delta$ LZ and  $\Delta$ CTD, that removed the LZ domain or the C terminus of CA, respectively. Single virion analysis results revealed that removal of the LZ domain had a slight effect on RNA packaging efficiency. However, removing only the CTD of CA ( $\Delta$ CTD)

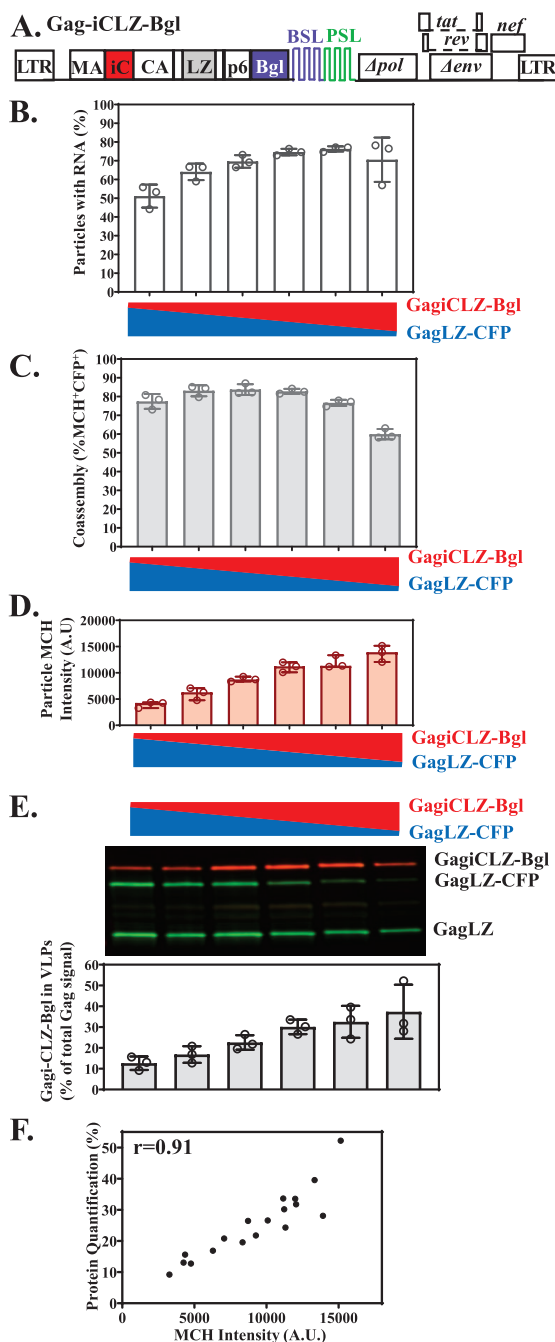


**FIG 2** Visualizing the RNA-binding Gag allows for correlation of MCH particle intensity with protein incorporation into viral particles. (A) General structure of Gag-iCLZ-Bgl. An internal mCherry (iC) was inserted between MA and CA domains (red). Other abbreviations are the same as in Fig. 1. (B) The percentage of particles containing PP7-YFP-labeled RNA. Of the Gag-encoding plasmids, GagLZ (77%) was transfected into 293T cells with increasing and decreasing amounts of Gag-iCLZ-Bgl (4 to 20%) and GagLZ-CFP (19 to 3%), respectively. The percentage of Gag-iCLZ-Bgl used in the titrations were 4, 7, 10, 15, 18, and 20%. (C) The percentage of Gag-iCLZ-Bgl coassembled into particles was calculated throughout the titration. The mean  $\pm$  standard deviation from three independent experiments is indicated. (D) Median MCH particle intensity in arbitrary units (A.U.) of coassembled particles is depicted as a median of three independent trials  $\pm$  95% confidence interval (95% CI). (E) Representative Western blot image of viral lysate probed with anti-p24 (green) and anti-MCH (red) antibodies. The positions of bands corresponding to Gag-iCLZ-Bgl, GagLZ-CFP, and GagLZ are indicated on the right. The percentage of Gag-iCLZ-Bgl relative to total Gag species packaged into particles as quantified by densitometry of Western blots from three independent experiments is shown below as the mean  $\pm$  standard deviation. Individual values from independent experiments are shown as open circles in each panel. (F) Correlation plot of the percentage of Gag-iCLZ-Bgl protein incorporated into particles versus the corresponding median MCH particle intensity for each experimental data point shown in panels D and E. The Pearson correlation coefficient is 0.91.

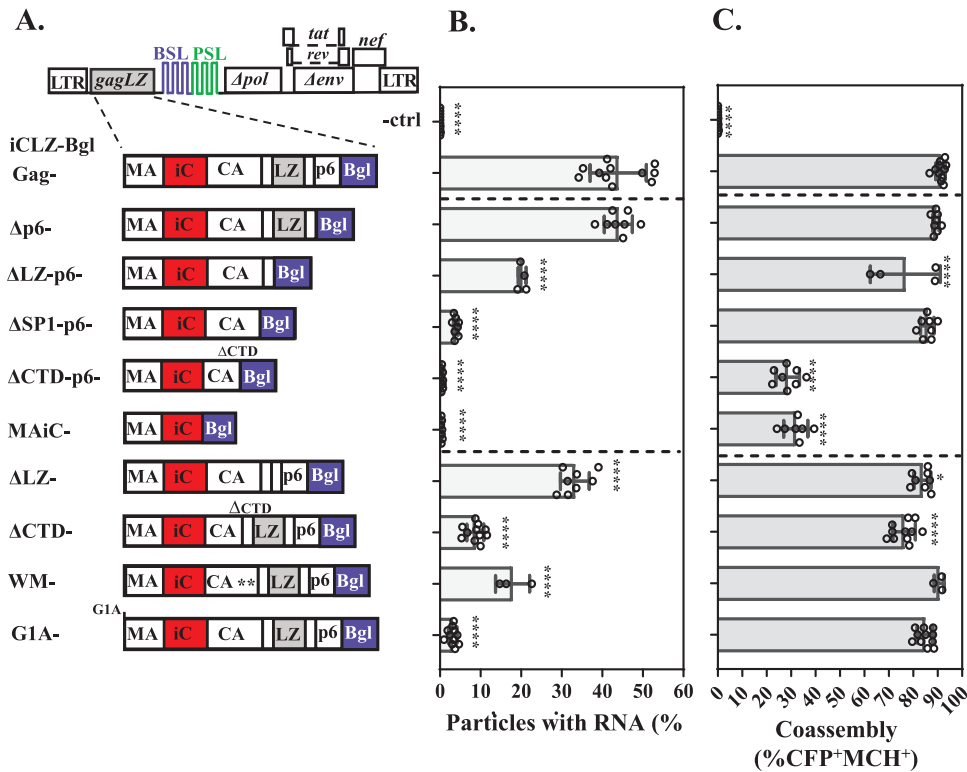


**FIG 3** Mutational analysis to determine features in HIV-1 Gag important for genome packaging and coassembly. (A) Schematic of deletion and point mutations made in Gag-iCLZ-Bgl. Amino acids 184 and 185 in CA of the WM mutant are denoted by two asterisks. GagLZ, GagLZ-CFP, and PP7-YFP alone (negative control) or with the indicated Gag-iCLZ-Bgl mutants were transfected into 293T cells, and viral particles were analyzed for RNA packaging efficiency (B) and coassembly (C). Dashed lines separate negative control (-ctrl) and Gag-iCLZ-Bgl from serial truncation mutants (middle) and single domain or point mutants (bottom). In these experiments, the ratios of GagLZ/GagLZ-CFP/Gag-iCLZ-Bgl constructs were 2:1:1 in all samples except in the negative control (-ctrl), in which GagLZ/GagLZ-CFP was 1:1. All samples were compared with results from Gag-iCLZ-Bgl. Statistical significance was evaluated by a one-way ANOVA with Bonferroni's multiple-comparison posttest and indicated as follows: \*,  $P < 0.05$ ; \*\*\*\*,  $P < 0.0001$ . Individual values from 3 to 11 independent trials are indicated by open circles. Bars indicate means  $\pm$  standard deviations.

generated a fivefold decrease in particles with viral RNA. To further examine the effects of Gag multimerization, we used a less severe oligomerization mutant, WM, in which methionine and tryptophan residues 184 and 185 in CA were substituted with alanine residues. The WM mutant has been shown to exhibit reduced Gag<sup>WM</sup>:Gag<sup>WM</sup> dimerization; however, Gag<sup>WM</sup> retains the ability to dimerize with wild-type (WT) Gag *in vitro* (23). We found that introducing these two point mutations caused a 2.5-fold decrease in genome packaging, further demonstrating the role of Gag multimerization in genome packaging. It is important to note that the WM mutation does not completely abolish the ability of Gag to multimerize, and mutants can assemble to make virus particles, albeit far less efficiently than wild-type Gag (24, 25). Therefore, the less severe decrease in RNA packaging observed with the WM mutant in comparison to ΔCTD could be a consequence of incomplete prevention of Gag multimerization.

HIV-1 assembly occurs at the plasma membrane where Gag multimerizes on viral RNAs. Gag targets and anchors to the plasma membrane using the myristoyl moiety posttranslationally added on the first glycine residue of MA (26). To examine whether the membrane targeting property of Gag is also important in genome packaging, we generated a substitution mutation that replaced the glycine residue with alanine (G1A), thereby causing a loss of myristylation and abolishing the ability of the mutant Gag to anchor to the plasma membrane. We found that the G1A mutation caused



severe defects in genome packaging, with a 14-fold decrease compared to that of Gag-iCLZ-Bgl and was statistically equivalent to the negative control (Fig. 3B).

The multidomain deletion mutants MAiCLZ-Bgl and  $\Delta$ CTD-p6-iCLZ-Bgl both displayed a threefold reduction in coassembled particles (Fig. 3C), making it difficult to determine whether the defect in RNA packaging could be due to reduced coassembly into particles. In contrast, the G1A-,  $\Delta$ CTD-, and WM-iCLZ-Bgl Gag proteins efficiently coassembled into particles, suggesting that the loss in RNA packaging does not stem from an inability to form viral particles with GagLZ-CFP. These results suggest that Gag must multimerize on the RNA while anchored at the plasma membrane for efficient HIV RNA packaging to occur.

**The RNA packaging defects displayed by G1A,  $\Delta$ CTD, and WM are independent of the amount of mutant proteins incorporated into viral particles.** Although G1A-,  $\Delta$ CTD-, and WM-iCLZ-Bgl coassemble into GagLZ/GagLZ-CFP particles, it was possible that a smaller amount of mutant proteins was incorporated into each particle, resulting in RNA packaging defects. Therefore, a more in-depth comparison of G1A-,  $\Delta$ CTD-, and WM-iCLZ-Bgl with the parent Gag-iCLZ-Bgl was carried out. As we previously determined that the MCH signal intensity in particles correlated with protein incorporation, we compared the RNA packaging efficiencies between samples with similar MCH intensities to accurately determine the RNA packaging capability of each mutant. GagLZ, GagLZ-CFP, and PP7-YFP were transfected with various concentrations of mutant or parent Gag-iCLZ-Bgl. Each mutant was able to coassemble efficiently under all tested conditions; over 70% of the particles contained both GagLZ-CFP and the RNA-binding GagLZ (Fig. 4A). Additionally, an incremental increase in median MCH particle intensity was observable for the parent Gag-iCLZ-Bgl and G1A-iCLZ-Bgl as each was titrated into the system. MCH intensities comparable with the parent Gag-iCLZ-Bgl were achieved for G1A-,  $\Delta$ CTD-, and WM-iCLZ-Bgl, as indicated by the paired symbols in Fig. 4B. Under conditions where G1A comprised 24% or 30% of the total GagLZ-encoding plasmids transfected into the system, the MCH particle intensity was similar to samples in which Gag-iCLZ-Bgl-expressing plasmid constituted 15% of the total GagLZ plasmid amount transfected into cells (Fig. 4B, open triangles). Particles produced from cells transfected with 24%  $\Delta$ CTD- or WM-iCLZ-Bgl had comparable MCH intensities to those produced with 15% and 20% Gag-iCLZ-Bgl, respectively (Fig. 4B, diamonds and squares). Importantly, even when the median MCH particle intensities for each mutant were equivalent to or higher than that of Gag-iCLZ-Bgl particles, RNA packaging by G1A-,  $\Delta$ CTD-, and WM-iCLZ-Bgl was not rescued (Fig. 4C). When comparing RNA packaging of paired columns as indicated, G1A-iCLZ-Bgl packaged RNA 11- to 37-fold less efficiently than Gag-iCLZ-Bgl. Mutant  $\Delta$ CTD-iCLZ-Bgl and WM-iCLZ-Bgl packaged RNA 6.5-fold and 2.2-fold less efficiently than the parent Gag-iCLZ-Bgl, respectively. In each case, the mutant RNA packaging ability is significantly impaired compared to Gag-iCLZ-Bgl (one-way analysis of variance [ANOVA] with Bonferroni's multiple-comparison posttest,  $P < 0.001$ ). Therefore, the RNA packaging defects displayed by myristylation and oligomerization mutants are independent of their ability to assemble into particles.

**Defining properties of Gag important for NC-mediated genome packaging.** The experiments described above demonstrate that the abilities of Gag to multimerize and anchor to the plasma membrane are important for genome packaging in the context of a nonviral RNA-binding protein. We adapted the complementation system to determine whether NC-mediated genome packaging requires the same Gag properties (Fig. 5). In this system, GagLZ and GagLZ-CFP were also used to produce viral particles, whereas RNA packaging is mediated by an NC-containing Gag (Fig. 5A). To ensure efficient coassembly, a LZ motif was added to the C terminus of Gag (CTLZ) and MCH was fused to the C terminus of the LZ motif to allow visualization of the protein, resulting in a Gag construct termed Gag-CTLZ-MCH (Fig. 5B). All of the Gag proteins were expressed from a NL4-3-derived construct containing an unmodified 5' untranslated region, which is known to be important for RNA packaging. Additionally, Gag-expressing constructs contained BSL stem-loop sequences recognized by BglG protein. In all

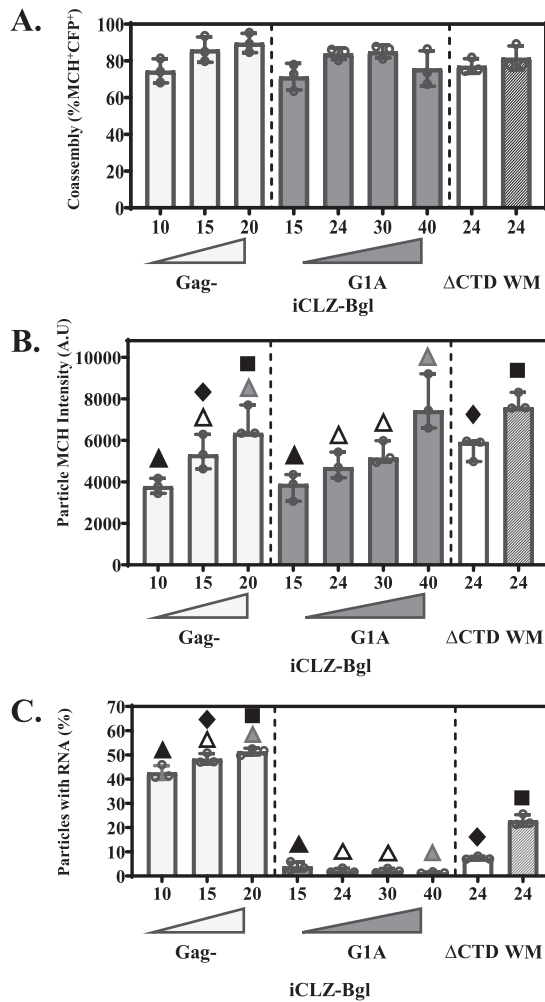


**FIG 4** Loss in RNA packaging is independent of mutant Gag incorporation. (A) Coassembly of Gag-iCLZ-Bgl and GagLZ-CFP are indicated as a percentage of total viral particles; bars represent the means  $\pm$  standard deviations. (B) Median MCH intensity of coassembled particles from three independent experiments with 95% CI. Paired symbols indicate median MCH intensities of similar values. Diamonds and squares denote conditions under which Gag- and  $\Delta$ CTD- or WM-iCLZ-Bgl particles display comparable MCH intensity, respectively. Filled, open, and gray triangles correspond to conditions in which Gag- and G1A-iCLZ-Bgl particles exhibit comparable MCH intensities. (C) The proportion of RNA-containing viral particles from cells transfected with GagLZ, GagLZ-CFP, PP7-YFP and various amounts of Gag-, G1A-,  $\Delta$ CTD-, or WM-iCLZ-Bgl is shown as the mean  $\pm$  standard deviation. One-way ANOVA with Bonferonni's multiple-comparisons posttest was used. (C) Symbols indicate statistical analysis of conditions in which MCH particle intensity are similar. Each paired symbol combination represents  $P < 0.0001$ . (A to C) Titrations of Gag- and G1A- are separated from each other and  $\Delta$ CTD- and WM-iCLZ-Bgl by dashed lines. The percentage of each iCLZ-Bgl plasmid transfected into cells is indicated on the x axis. Individual values from three independent experiments are shown as open circles.

experiments, a plasmid expressing a YFP-tagged BglG protein (Bgl-YFP) was coexpressed. Thus, in this system, assembly of GagLZ and GagLZ-CFP generates CFP<sup>+</sup> particles, coassembly of Gag-CTLZ-MCH generates CFP<sup>+</sup> MCH<sup>+</sup> particles, and if RNA-binding Gag can recruit Bgl-YFP-labeled HIV-1 RNA, CFP<sup>+</sup> MCH<sup>+</sup> YFP<sup>+</sup> particles can be generated. These constructs were transfected into cells, and particles were harvested and analyzed. In these transfections, GagLZ was maintained at the same level (55% of the Gag-expressing plasmids) in all samples, whereas the GagLZ-CFP and NC-containing Gag were varied. We found that Gag-CTLZ-MCH can be coassembled into CFP<sup>+</sup> particles (Fig. 6A and B); furthermore, viral RNA can be packaged into particles (Fig. 6C).

We used a  $\Delta$ p6 mutant to test whether GagLZ and GagLZ-CFP could rescue NC-containing Gag constructs. Deletion of the p6 domain is known to severely inhibit HIV-1

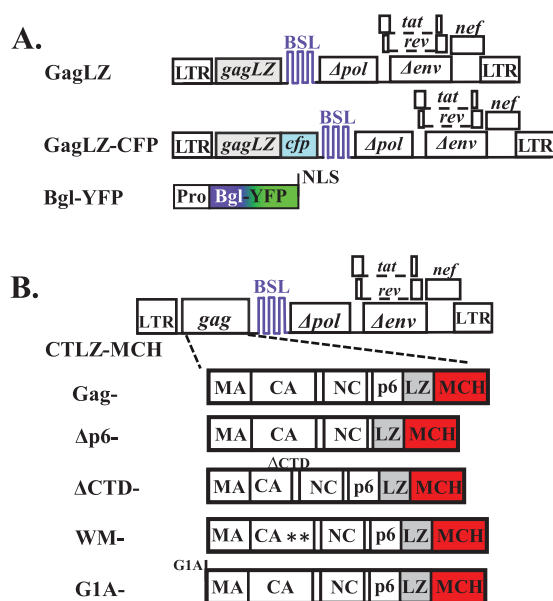


**FIG 5** NC-dependent packaging system. (A) General structures of constructs used to express GagLZ, GagLZ-CFP, and Bgl-YFP. (B) NC-containing Gag constructs. Parent construct in which each Gag-CTLZ-MCH mutant was made is depicted at top, followed by schematics of Gag-CTLZ-MCH and mutants. A LZ domain (gray) and a mCherry fluorescent protein (MCH) were fused to the C terminus of Gag. Point mutations made at amino acids 184 and 185 in CA of the WM mutant are denoted by asterisks. All constructs contain a set of stem-loop sequences, BSL (purple), inserted into *pol* which are recognized by Bal-YFP.

particle release. In our NC-independent BglG-mediated packaging system described above, deleting the p6 domain did not affect RNA packaging (Fig. 3). Therefore, Δp6-CTLZ-MCH is expected to coassemble with GagLZ and GagLZ-CFP and packaged the RNA genome. We found that when transfected with GagLZ and GagLZ-CFP, Δp6-CTLZ-MCH protein was assembled into particles efficiently (Fig. 6A). The MCH particle intensity of Δp6 (15%; square) matched that of Gag-CTLZ-MCH (15%); furthermore, Δp6 packaged RNA at efficiencies similar to that of Gag-CTLZ-MCH (Fig. 6B and C). These results confirmed that the system is capable of rescuing Gag mutants with defects in particle production.

To examine whether anchoring Gag to the plasma membrane is an important property for NC-mediated genome packaging, we introduced the G1A mutation in Gag-CTLZ-MCH and performed single virion analysis with increasing amounts of the RNA-binding Gag. As shown in Fig. 6A, G1A-CTLZ-MCH efficiently coassembled into CFP<sup>+</sup> particles; however, it failed to incorporate RNA genome into the particles (Fig. 6C). The efficiency of genome packaging was not statistically different from the negative-control sample lacking any RNA-binding Gag ( $P > 0.9999$ , one-way ANOVA with Bonferonni's multiple-comparison posttest; Fig. 6C). We observed that, compared to Gag-CTLZ-MCH, G1A-CTLZ-MCH proteins do not coassemble into the CFP particles as efficiently, which is evidenced by a decreased relative median MCH fluorescence particle intensity (Fig. 6B). However, higher levels of G1A-CTLZ-MCH protein incorporation were achieved when we increased the ratio of the G1A mutant plasmid in the total Gag-expressing plasmids (Fig. 6B). Comparing the RNA packaging efficiencies between samples with similar MCH particle intensities indicated that similar levels of RNA-binding Gag were coassembled into the viruses. These samples are indicated by paired symbols in Fig. 6B and C. For example, when 10% and 40% of the Gag-expressing plasmids encoded Gag-CTLZ-MCH and G1A-CTLZ-MCH, particles from these two samples have similar MCH intensities (indicated by gray triangles). Thus, we compared the RNA packaging efficiencies between G1A-CTLZ-MCH (40%) and Gag-CTLZ-MCH (10%) and found that the G1A mutant packages the RNA

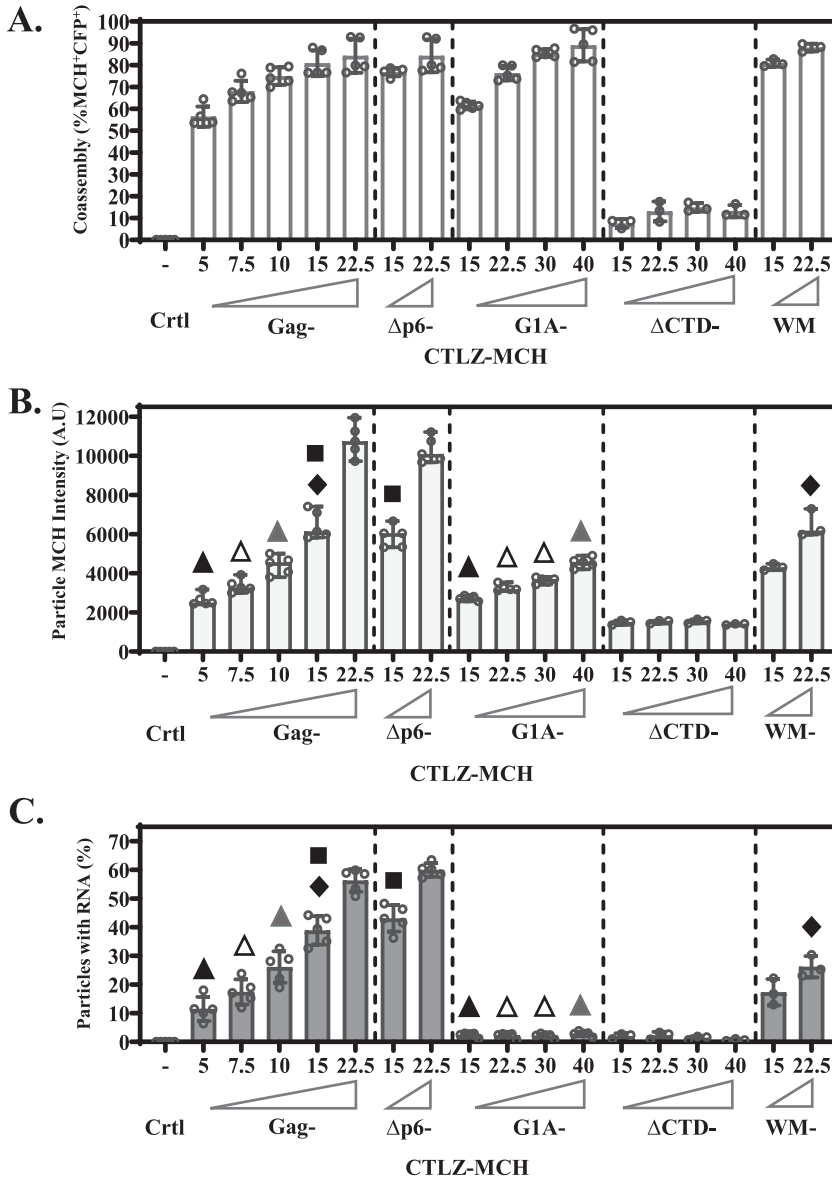


**FIG 6** NC-dependent RNA packaging requires functional Gag plasma membrane anchoring and multimerization. (A to C) GagLZ, GagLZ-CFP, Bgl-YFP alone (negative control [- Ctrl]) or along with Gag-CTLZ-MCH mutants were transfected into cells and viral particles analyzed for coassembly of Gag proteins (A), MCH particle intensity (B), and RNA packaging (C). The mean ± standard deviation (A and C) or median with 95% CI (B) is shown. Individual values from three to five independent experiments are indicated by open circles. The percentage of each Gag-CTLZ-MCH among the total Gag-encoding plasmids transfected into cells is indicated on the x axis. Gag-, Δp6-, G1A, ΔCTD-, and WM -CTLZ-MCH samples are separated by dashed lines. One-way ANOVA with Bonferroni’s multiple comparisons posttest was used. Symbols indicate statistical analysis of conditions in which MCH particle intensity are similar. RNA packaging efficiencies between Gag-CTLZ-MCH and mutants in filled triangles ( $P < 0.01$ ), diamond ( $P < 0.001$ ), empty and gray triangles ( $P < 0.0001$ ), square (not significant [ns]).

genome at a ninefold-lower efficiency compared to Gag-CTLZ-MCH ( $P < 0.0001$ ). Similarly, RNA packaging in G1A-CTLZ-MCH (22.5 or 30%; open triangles) is eightfold less efficient than Gag-CTLZ-MCH (7.5%), respectively ( $P < 0.001$ ). These results indicate that even when similar amounts of G1A mutant proteins are coassembled into particles, they exhibit a significant defect in genome packaging.

To investigate whether the ability of Gag to multimerize is important for NC-mediated RNA genome packaging, we introduced the ΔCTD and WM mutations into Gag-CTLZ-MCH. Single virion analysis results showed that the ΔCTD-CTLZ-MCH did not

efficiently coassemble into CFP particles and did not package viral RNA (Fig. 6,  $\Delta$ CTD). On the basis of these results, we could not distinguish between a defect in Gag coassembly and a defect in RNA packaging. We then studied the WM mutant and found that it is efficiently coassembled into particles (Fig. 6A). We then compared the MCH intensities among particles coassembled with WM- or Gag-CTLZ-MCH and found that WM-CTLZ-MCH (22.5%) particles have similar MCH intensities as Gag-CTLZ-MCH (15%) (Fig. 6B). However, the genome packaging in WM (22.5%) is 1.5-fold lower than the WT (15%) (Fig. 6C, diamonds), which is significant ( $P < 0.001$ ).

## DISCUSSION

HIV-1 Gag orchestrates complex interactions with viral and cellular components to assemble infectious viruses. One of the key steps is the packaging of RNA genome that carries the genetic information essential for future rounds of viral replication. Only a small fraction of the cellular RNA is HIV-1 RNA; furthermore, Gag binds only HIV-1 RNA with slight preference in the cytoplasm. Thus, it is unclear how the highly efficient HIV-1 genome packaging is achieved. Gag:RNA genome interactions are complex and constitute different types of interactions. We have previously hypothesized that genome packaging is the nucleation point of HIV-1 assembly and have shown that the presence of HIV-1 RNA enhances Gag assembly (4, 27). We posit that the initial Gag:RNA interactions are specific and such Gag:RNA complexes nucleate the assembly process by facilitating subsequent Gag recruitment. In contrast, Gag recruited at later stages of assembly largely interacts with viral RNA in a nonspecific manner. In this report, we focused on the initial Gag:RNA interactions that nucleate the assembly complex and package the viral RNA genome. For this purpose, we developed complementation systems that separate two functions of the Gag protein: particle production and genome packaging. These systems used a combination of assembly-competent Gag and RNA-binding Gag that can package the viral genome into approximately half of the particles. We mutated the RNA-binding Gag and identified Gag mutants that can coassemble into particles but could not package RNA. Using this strategy, we demonstrated that, in addition to RNA binding, the capacities for Gag to anchor at the plasma membrane and mediate Gag:Gag multimerization are two important properties in genome packaging (Fig. 7).

Multimerization of Gag is essential at several stages of the viral replication cycle. During assembly, Gag multimerizes at the plasma membrane eventually leading to the formation of immature virus particles. The C-terminal domain of CA contains the major homology region (MHR) and helix 9, which serves as a dimeric interface between Gag molecules (7). The CA-CTD has also been suggested to play a role in stabilizing Gag:RNA interactions (28). Using GagLZ fused to a nonviral RNA-binding protein, we showed that removal of CA-CTD did not abolish the capacity of the mutant Gag to be coassembled into particles but significantly interfered with genome packaging. This finding suggests that the CA-CTD may not be stabilizing direct binding to the RNA but is essential for efficient RNA packaging. Changing the 184 and 185 residues within the CA-CTD to alanine resulted in the WM mutant with Gag multimerization defects and decreased particle production compared with wild-type virus (23, 24, 29). We observed a mild, but significant, 2.5-fold decrease in the capacity of WM-iCLZ-Bgl to package HIV-1 RNA. Additionally, we have also examined genome packaging using the HIV-1 NC-mediated RNA interaction and found that the WM mutant also exhibited a 1.5-fold defect in genome packaging. Taken together, our results indicate the presence of the RNA-binding Gag in the virus particle is necessary but not sufficient for efficient genome packaging. Genome packaging requires not only the RNA-binding Gag proteins to bind HIV-1 RNA but also multimerize among these RNA-binding Gag proteins.

Our results also showed that the G1A mutant exhibited severe RNA packaging defects. Mutation of the first glycine to alanine in MA prevents myristylation of Gag, resulting in loss of anchoring to the plasma membrane and particle production (26). G1A mutant Gag proteins are diffuse within the cytoplasm and do not assemble (30).

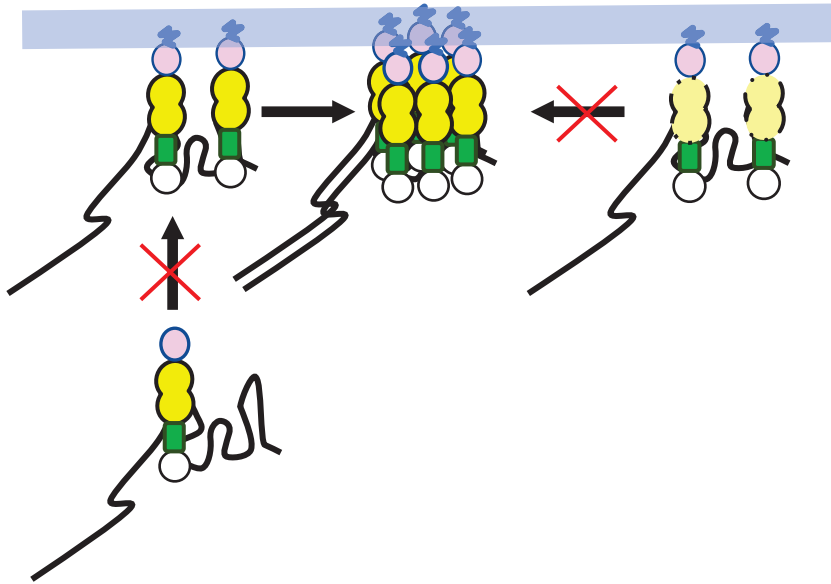


**FIG 7** Proposed model for HIV-1 RNA packaging. Wild-type Gag proteins bind viral RNA (black line) at the plasma membrane (shown as light blue area) (top left). To package RNA, Gag proteins must multimerize on viral RNA to form stable complex (top center). Gag with multimerization defects (top right) and Gag with membrane anchoring defects (bottom) cannot form stable Gag:viral RNA complex, resulting in genome packaging defects. Two copies of viral RNA are shown in the stable complex; however, for the BglG-mediated genome packaging, the number of RNA genomes in a particle is not known.

In previous studies, mutations in the MA domain resulting in mislocalization of assembly could be rescued when WT Gag was supplied in *trans* (31). It has been shown that the G1A mutation does not alter the ability of Gag to bind viral RNA because wild-type Gag and G1A Gag bind viral RNA in a similar manner and efficiency in the cytoplasm (16, 28). Therefore, it was possible that the G1A mutant Gag proteins could bind to viral RNA and interact with GagLZ proteins capable of anchoring to the plasma membrane to generate particles containing RNA genomes. However, RNA-binding G1A Gag exhibits a severe genome packaging defect even though it can coassemble into the particles. These results indicate that the Gag:RNA interactions that lead to nucleation of the assembly complex occur at the plasma membrane. Lacking its own myristylation signal, G1A can remain at the plasma membrane only by interacting with GagLZ that has a myristylation signal. Because each RNA-binding G1A Gag must interact with at least one GagLZ to remain at the plasma membrane, it is difficult for G1A Gag to multimerize among themselves on the viral RNA to form the nucleation complex. Indeed, in BglG- and NC-mediated RNA packaging systems, the G1A mutant has a severe RNA packaging defect; the efficiencies of RNA packaging are not significantly different from those of negative controls.

The results of this study indicate that Gag proteins bind to viral RNA and multimerize to form a stable complex at the plasma membrane to package the genome (Fig. 7). Mutations in Gag that affect membrane anchoring or multimerization cause packaging defects. Using a reverse-footprinting approach, multiple NC binding sites have been mapped in the HIV-1 5' UTR *in vivo* (32). Mutations at these sites affect Gag binding and genome packaging efficiencies (15, 33). Furthermore, mutating two binding sites caused little or no defect, whereas combining multiple NC binding site mutations cause synergistic defects (33). Taken together, these studies suggest that during the assembly process, Gag interacts with viral RNA at the plasma membrane. During this process, Gag proteins bind to multiple sites in the 5' UTR of HIV-1 RNA, promoting Gag-Gag multimerization, and nucleate the assembly complex (Fig. 7). After the formation of the initial nucleation complex, additional Gag proteins join the complex and mostly

interact with RNA in a nonspecific manner. The G1A,  $\Delta$ CTD, and WM mutants are defective at forming the nucleation complex but can join the complex at a later stage, thereby exhibiting coassembly competent phenotype but unable to package RNA efficiently.

In this report, we describe two complementation systems that can be used to study viral assembly. For example, it has been reported that the p6 domain contributes to RNA packaging (34) although this has been refuted by another study that found that p6-deleted Gag binds RNA efficiently (35). Because deletion of the p6 domain severely inhibits particle release, it is difficult to study the effects of p6 deletion on virion RNA content (36). In our complementation systems, this block in particle budding was rescued, and we confirmed that removal of the p6 domain had no impact on RNA genome packaging in either a NC-independent or -dependent system. Thus, these systems can be used to study other aspects of virus assembly.

## MATERIALS AND METHODS

**HIV-1 constructs and RNA-binding protein plasmids.** Constructs Gag-BSL-PSL and GagCFP-BSL-PSL express Gag and CFP-tagged Gag, respectively. A DNA fragment containing PSL, 24 copies of stem-loop sequences recognized by PP7 coat protein (37), were inserted into previously described 1-Gag-BSL, and 1-GagCFP-BSL (11) to generate Gag-BSL-PSL and GagCFP-BSL-PSL, respectively. Similarly, PSL was added to 1-GagLZ-BSL and 1-GagLZCFP-BSL (38) to generate GagLZ-BSL-PSL and GagLZCFP-BSL-PSL, respectively. Construct GagLZ-Bgl-BSL-PSL is similar to GagLZ-BSL-PSL with a DNA fragment encoding the RNA-binding domain of BglG added to the end of GagLZ. The plasmid expressing Gag-iC-LZ-Bgl-BSL-PSL was generated in a two-step process. First, a DNA fragment encoding MCH was used to replace that of an internal green fluorescence protein (iGFP) in the previously described pNL4-3 iGFP  $\Delta$ env (21) to generate an iC-containing pNL4-3 iC  $\Delta$ env. Then, an AatII-to-NsiI fragment encompassing MCH from pNL4-3 iC  $\Delta$ env was used to replace the counterpart in GagLZ-Bgl-BSL-PSL to generate Gag-iCLZ-Bgl-BSL-PSL. Truncation or deletion mutants of Gag-iCLZ-Bgl-BSL-PSL shown in Fig. 3 were generated by replacing the NsiI-to-XmaI fragment of the plasmids with synthesized DNA fragments containing the deletions (IDT). A DNA fragment containing the G1A mutation in MA was synthesized (IDT) and used to replace the BssHII-to-MluI fragment in the pNL4-3iC  $\Delta$ env to generate NL4-3 G1AiC  $\Delta$ env. A region containing the G1A mutation was then amplified from NL4-3 G1AiC  $\Delta$ env and used to replace the AatII-to-SgrAI fragment in Gag-iCLZ-Bgl-BSL-PSL to generate G1A-iCLZ-Bgl-BSL-PSL. To generate G1A-MCH-BSL, a SphI-to-MluI DNA fragment containing the G1A mutation from the previously described pNL4-3 1GA (myr-) (26) was used to replace the corresponding region in GagMCH-BSL (39). Overlapping PCR was performed to delete the CTD of CA (40) from GagMCH-BSL to generate  $\Delta$ CTD-MCH-BSL. A DNA fragment containing the  $\Delta$ p6 deletion was synthesized (IDT) and replaced the SphI-to-XmaI fragment in GagMCH-BSL to generate  $\Delta$ p6Gag-MCH-BSL. A DNA fragment encoding a LZ motif with short linkers flanking each side was synthesized (IDT) and inserted between the C terminus of Gag and MCH of G1AGagMCH-BSL,  $\Delta$ CTDGagMCH-BSL,  $\Delta$ p6GagMCH-BSL, and GagMCH-BSL to generate G1A-,  $\Delta$ CTD-,  $\Delta$ p6-, and Gag-CTLZ-MCH-BSL, respectively. A DNA fragment containing the WM 184,185 amino acid (AA) mutation was amplified by PCR from pNL-MA-WM184\_185AA (29) and used to replace the SphI-to-XmaI fragment of GagMCH-BSL to generate WMGagMCH-BSL, followed by insertion of CTLZ to create WM-CTLZ-MCH-BSL.

Plasmids MS2-mKate and Bgl-YFP have been previously described (39, 41). Plasmid PP7-YFP was based on a previously described plasmid (42) except the green fluorescent protein tag of tandem PP7 coat protein was replaced with YFP. Plasmid Bgl-mKate is similar to Bgl-YFP; however, the BglG RNA-binding domain is tagged with mKate fluorescent protein (20). Molecular cloning was performed by using standard methods. The general structures of the plasmids were confirmed by restriction mapping, and regions that were amplified by PCR were confirmed by DNA sequencing.

**Cell culture and single virion analysis.** Human embryonic kidney 293T cells were maintained in Dulbecco's modified Eagle's medium supplemented with 10% fetal bovine serum, 50 U/ml penicillin, and 50  $\mu$ g/ml streptomycin. Cells were cultured in a humidified 37°C incubator with 5% CO<sub>2</sub>. Transfections were performed using FuGENE HD (Promega) transfection reagent according to the manufacturer's protocol with a ratio of 1  $\mu$ l of reagent to 4 total  $\mu$ g of DNA. In all experiments, plasmids expressing unlabeled GagLZ comprised more than 50% of the total Gag-expressing DNA, whereas plasmids encoding GagLZ-CFP and the RNA-binding Gag varied. In the competition assay, Bgl-mKate and MS2-mKate concentrations were varied from 0 to 1,500 ng in transfection samples. In all assays, 750 ng of Bgl-YFP or PP7-YFP was transfected in each sample to label viral RNA.

Supernatants were harvested 24 h posttransfection, filtered through a 0.45- $\mu$ m syringe filter (Millipore) to remove cellular debris, and either aliquoted and stored at -80°C, imaged immediately, or processed for immunoblotting. Single virion analysis was carried out as previously described (11). Briefly, supernatants were diluted in phosphate-buffered saline on  $\mu$ -Slide ibiTreat eight-well slides (Ibidi) with Polybrene (50  $\mu$ g/ml, final concentration) and spun in a Beckman Coulter Allegra 21R with a Beckman Coulter S2096 rotor for 1 h at 1,200  $\times$  g prior to fluorescence microscopy imaging. Epifluorescence microscopy images were captured using an inverted Nikon Eclipse TE 2000 microscope and a 100 $\times$  1.49-numerical-aperture oil objective, with a SOLA light engine light source (Lumencor) for illumination. Digital images were acquired

using a Hamamatsu ORCA-ERA camera and NIS-Elements software (Nikon) with the excitation and emission filter sets 427/10 nm and 472/30 nm for CFP, 504/12 nm and 542/27 nm for YFP, and 577/25 nm and 632/60 nm for MCH. The diffraction-limited spots were detected, and their positions were determined in each image using Localize (43). A minimum of 1,000 particles were analyzed for each condition in every experiment. Colocalization and intensities of the GagLZ (CFP), RNA (YFP), and RNA-binding Gag (MCH) signals were determined using a custom MATLAB program (Mathworks) (11, 44); signals were considered colocalized if their centers were within 3 pixels ( $\sim 0.39 \mu\text{m}$ ).

RNA packaging efficiency was calculated by determining the fraction of triple positive (CFP<sup>+</sup> YFP<sup>+</sup> MCH<sup>+</sup>) particles among CFP<sup>+</sup> particles in all cases except in instances when MCH containing Gag was absent, in which case packaging efficiency was defined as the percentage of dual positive (CFP<sup>+</sup> YFP<sup>+</sup>) particles among CFP<sup>+</sup> particles. Coassembly was calculated as the percentage of dual positive (CFP<sup>+</sup> MCH<sup>+</sup>) particles among total particles (CFP<sup>+</sup> or MCH<sup>+</sup>). One-way ANOVA multiple-comparison tests with Bonferroni correction and correlation analysis were performed using GraphPad Prism version 8.4.3 for Windows (GraphPad Software, La Jolla, CA, USA, [www.graphpad.com](http://www.graphpad.com)).

**Western blotting.** Filtered supernatants were centrifuged at  $15,000 \times g$  for 2 h at 4°C through a 20% sucrose cushion, aspirated, and resuspended in phosphate-buffered saline (PBS) with an appropriate volume of 4× Laemmli sample buffer (Bio-Rad) containing 10% beta-mercaptoethanol. Viral lysate samples were incubated at 99°C for 5 min. Sodium dodecyl sulfate-polyacrylamide gel electrophoresis (SDS-PAGE) was performed using 4 to 20% Criterion TGX precast gels (Bio-Rad), transferred to polyvinylidene difluoride (PVDF) membranes, and probed with rabbit anti-mCherry (NovusBio catalog no. NBP2-43720; 1:3,000) and mouse anti-HIVp24 (NIH AIDS Reagent Program, Division of AIDS, NIAID, NIH, HIV-1 p24 Gag Monoclonal [24-3] from Michael H. Malim catalog no. 6458; 1:3,000). These were followed with incubation of either goat anti-mouse IgG (IRDye 680CW; Li-Cor) or goat anti-rabbit IgG (IRDye 800RD; Li-Cor) secondary antibodies at 1:10,000 dilutions. Western blots were imaged and quantified using the Odyssey CLx infrared imaging system and Image Studio Lite v5.2 (Li-Cor). To calculate the percentage of packaged Gag-iC-LZ-Bgl, background-subtracted intensities of Gag-iC-LZ-Bgl bands were divided by the sum intensities of all Gag (p24) bands. Three independent blots were performed.

## ACKNOWLEDGMENTS

This work was supported by the Intramural Research Program of the National Institutes of Health (NIH), National Cancer Institute (NCI), Center for Cancer Research, by an NIH Intramural AIDS Research Fellowship (to A.D.), NIH Intramural AIDS Targeted Antiviral Program grant funding (to W.-S.H. and to V.K.P.), and by the Innovation Fund, Office of AIDS Research, NIH (to W.-S.H. and to V.K.P.).

## REFERENCES

- Freed EO. 2015. HIV-1 assembly, release and maturation. *Nat Rev Microbiol* 13:484–496. <https://doi.org/10.1038/nrmicro3490>.
- Kuzembayeva M, Dilley K, Sardo L, Hu WS. 2014. Life of psi: how full-length HIV-1 RNAs become packaged genomes in the viral particles. *Virology* 454-455:362–370. <https://doi.org/10.1016/j.virol.2014.01.019>.
- Rein A. 2019. RNA packaging in HIV. *Trends Microbiol* 27:715–723. <https://doi.org/10.1016/j.tim.2019.04.003>.
- Nikolaitchik OA, Dilley KA, Fu W, Gorelick RJ, Tai SH, Soheilian F, Ptak RG, Nagashima K, Pathak VK, Hu WS. 2013. Dimeric RNA recognition regulates HIV-1 genome packaging. *PLoS Pathog* 9:e1003249. <https://doi.org/10.1371/journal.ppat.1003249>.
- Schur FK, Obr M, Hagen WJ, Wan W, Jakobi AJ, Kirkpatrick JM, Sachse C, Kräusslich HG, Briggs JA. 2016. An atomic model of HIV-1 capsid-SP1 reveals structures regulating assembly and maturation. *Science* 353:506–508. <https://doi.org/10.1126/science.aaf9620>.
- Wagner JM, Zadrozny KK, Chrustowicz J, Purdy MD, Yeager M, Ganser-Pornillos BK, Pornillos O. 2016. Crystal structure of an HIV assembly and maturation switch. *Elife* 5:e17063. <https://doi.org/10.7554/eLife.17063>.
- Novikova M, Zhang Y, Freed EO, Peng K. 2019. Multiple roles of HIV-1 capsid during the virus replication cycle. *Virology* 544:119–134. <https://doi.org/10.1007/s12250-019-00095-3>.
- Zhang Y, Barklis E. 1997. Effects of nucleocapsid mutations on human immunodeficiency virus assembly and RNA encapsidation. *J Virol* 71:6765–6776. <https://doi.org/10.1128/JVI.71.9.6765-6776.1997>.
- Ott DE, Coren LV, Chertova EN, Gagliardi TD, Nagashima K, Sowder RC, II, Poon DT, Gorelick RJ. 2003. Elimination of protease activity restores efficient virion production to a human immunodeficiency virus type 1 nucleocapsid deletion mutant. *J Virol* 77:5547–5556. <https://doi.org/10.1128/jvi.77.10.5547-5556.2003>.
- Crist RM, Datta SA, Stephen AG, Soheilian F, Mirro J, Fisher RJ, Nagashima K, Rein A. 2009. Assembly properties of human immunodeficiency virus type 1 Gag-leucine zipper chimeras: implications for retrovirus assembly. *J Virol* 83:2216–2225. <https://doi.org/10.1128/JVI.02031-08>.
- Chen JB, Nikolaitchik O, Singh J, Wright A, Bencsics CE, Coffin JM, Ni N, Lockett S, Pathak VK, Hu WS. 2009. High efficiency of HIV-1 genomic RNA packaging and heterozygote formation revealed by single virion analysis. *Proc Natl Acad Sci U S A* 106:13535–13540. <https://doi.org/10.1073/pnas.0906822106>.
- Clever J, Sassetti C, Parslow TG. 1995. RNA secondary structure and binding sites for gag gene products in the 5' packaging signal of human immunodeficiency virus type 1. *J Virol* 69:2101–2109. <https://doi.org/10.1128/JVI.69.4.2101-2109.1995>.
- Comas-Garcia M, Datta SA, Baker L, Varma R, Gudla PR, Rein A. 2017. Dissection of specific binding of HIV-1 Gag to the 'packaging signal' in viral RNA. *Elife* 6:e27055. <https://doi.org/10.7554/eLife.27055>.
- Webb JA, Jones CP, Parent LJ, Rouzina I, Musier-Forsyth K. 2013. Distinct binding interactions of HIV-1 Gag to Psi and non-Psi RNAs: implications for viral genomic RNA packaging. *RNA* 19:1078–1088. <https://doi.org/10.1261/rna.038869.113>.
- Rye-McCurdy TD, Nadarai-Hoke S, Gudleski-O'Regan N, Flanagan JM, Parent LJ, Musier-Forsyth K. 2014. Mechanistic differences between nucleic acid chaperone activities of the Gag proteins of Rous sarcoma virus and human immunodeficiency virus type 1 are attributed to the MA domain. *J Virol* 88:7852–7861. <https://doi.org/10.1128/JVI.00736-14>.
- Kutluay SB, Zang T, Blanco-Melo D, Powell C, Jannain D, Errando M, Bieniasz PD. 2014. Global changes in the RNA binding specificity of HIV-1 gag regulate virion genesis. *Cell* 159:1096–1109. <https://doi.org/10.1016/j.cell.2014.09.057>.
- Houman F, Diaz-Torres MR, Wright A. 1990. Transcriptional antitermination in the bgl operon of E. coli is modulated by a specific RNA binding protein. *Cell* 62:1153–1163. [https://doi.org/10.1016/0092-8674\(90\)90392-r](https://doi.org/10.1016/0092-8674(90)90392-r).



18. Larson DR, Johnson MC, Webb WW, Vogt VM. 2005. Visualization of retrovirus budding with correlated light and electron microscopy. *Proc Natl Acad Sci U S A* 102:15453–15458. <https://doi.org/10.1073/pnas.0504812102>.
19. Chao JA, Patskovsky Y, Almo SC, Singer RH. 2008. Structural basis for the coevolution of a viral RNA-protein complex. *Nat Struct Mol Biol* 15:103–105. <https://doi.org/10.1038/nsmb1327>.
20. Shcherbo D, Merzlyak EM, Chepurnykh TV, Fradkov AF, Ermakova GV, Solovieva EA, Lukyanov KA, Bogdanova EA, Zaraisky AG, Lukyanov S, Chudakov DM. 2007. Bright far-red fluorescent protein for whole-body imaging. *Nat Methods* 4:741–746. <https://doi.org/10.1038/nmeth1083>.
21. Hübner W, Chen P, Del Portillo A, Liu Y, Gordon RE, Chen BK. 2007. Sequence of human immunodeficiency virus type 1 (HIV-1) Gag localization and oligomerization monitored with live confocal imaging of a replication-competent, fluorescently tagged HIV-1. *J Virol* 81:12596–12607. <https://doi.org/10.1128/JVI.01088-07>.
22. Li C, Burdick RC, Nagashima K, Hu WS, Pathak VK. 2021. HIV-1 cores retain their integrity until minutes before uncoating in the nucleus. *Proc Natl Acad Sci U S A* 118:e2019467118. <https://doi.org/10.1073/pnas.2019467118>.
23. Datta SA, Zhao Z, Clark PK, Tarasov S, Alexandratos JN, Campbell SJ, Kvaratskhelia M, Lebowitz J, Rein A. 2007. Interactions between HIV-1 Gag molecules in solution: an inositol phosphate-mediated switch. *J Mol Biol* 365:799–811. <https://doi.org/10.1016/j.jmb.2006.10.072>.
24. Datta SA, Curtis JE, Ratcliff W, Clark PK, Crist RM, Lebowitz J, Krueger S, Rein A. 2007. Conformation of the HIV-1 Gag protein in solution. *J Mol Biol* 365:812–824. <https://doi.org/10.1016/j.jmb.2006.10.073>.
25. Joshi A, Nagashima K, Freed EO. 2006. Mutation of dileucine-like motifs in the human immunodeficiency virus type 1 capsid disrupts virus assembly, Gag-Gag interactions, Gag-membrane binding, and virion maturation. *J Virol* 80:7939–7951. <https://doi.org/10.1128/JVI.00355-06>.
26. Freed EO, Orenstein JM, Buckler-White AJ, Martin MA. 1994. Single amino acid changes in the human immunodeficiency virus type 1 matrix protein block virus particle production. *J Virol* 68:5311–5320. <https://doi.org/10.1128/JVI.68.8.5311-5320.1994>.
27. Dilley KA, Nikolaitchik OA, Galli A, Burdick RC, Levine L, Li K, Rein A, Pathak VK, Hu WS. 2017. Interactions between HIV-1 Gag and viral RNA genome enhance virion assembly. *J Virol* 91:e02319–16. <https://doi.org/10.1128/JVI.02319-16>.
28. Kutluay SB, Bieniasz PD. 2010. Analysis of the initiating events in HIV-1 particle assembly and genome packaging. *PLoS Pathog* 6:e1001200. <https://doi.org/10.1371/journal.ppat.1001200>.
29. Ono A, Waheed AA, Joshi A, Freed EO. 2005. Association of human immunodeficiency virus type 1 Gag with membrane does not require highly basic sequences in the nucleocapsid: use of a novel Gag multimerization assay. *J Virol* 79:14131–14140. <https://doi.org/10.1128/JVI.79.22.14131-14140.2005>.
30. Inlora J, Chukkapalli V, Bedi S, Ono A. 2016. Molecular determinants directing HIV-1 Gag assembly to virus-containing compartments in primary macrophages. *J Virol* 90:8509–8519. <https://doi.org/10.1128/JVI.01004-16>.
31. Ono A, Orenstein JM, Freed EO. 2000. Role of the Gag matrix domain in targeting human immunodeficiency virus type 1 assembly. *J Virol* 74:2855–2866. <https://doi.org/10.1128/jvi.74.6.2855-2866.2000>.
32. Wilkinson KA, Gorelick RJ, Vasa SM, Guex N, Rein A, Mathews DH, Giddings MC, Weeks KM. 2008. High-throughput SHAPE analysis reveals structures in HIV-1 genomic RNA strongly conserved across distinct biological states. *PLoS Biol* 6:e96. <https://doi.org/10.1371/journal.pbio.0060096>.
33. Nikolaitchik OA, Somoulay X, Rawson JMO, Yoo JA, Pathak VK, Hu WS. 2020. Unpaired guanosines in the 5' untranslated region of HIV-1 RNA act synergistically to mediate genome packaging. *J Virol* 94:e00439–20. <https://doi.org/10.1128/JVI.00439-20>.
34. Dubois N, Khoo KK, Ghossein S, Seissler T, Wolff P, McKinstry WJ, Mak J, Paillart JC, Marquet R, Bernacchi S. 2018. The C-terminal p6 domain of the HIV-1 Pr55(Gag) precursor is required for specific binding to the genomic RNA. *RNA Biol* 15:923–936. <https://doi.org/10.1080/15476286.2018.1481696>.
35. Sarni S, Biswas B, Liu S, Olson ED, Kitzrow JP, Rein A, Wysocki VH, Musier-Forsyth K. 2020. HIV-1 Gag protein with or without p6 specifically dimerizes on the viral RNA packaging signal. *J Biol Chem* 295:14391–14401. <https://doi.org/10.1074/jbc.RA120.014835>.
36. Demirov DG, Orenstein JM, Freed EO. 2002. The late domain of human immunodeficiency virus type 1 p6 promotes virus release in a cell type-dependent manner. *J Virol* 76:105–117. <https://doi.org/10.1128/jvi.76.1.105-117.2002>.
37. Wu B, Chao JA, Singer RH. 2012. Fluorescence fluctuation spectroscopy enables quantitative imaging of single mRNAs in living cells. *Biophys J* 102:2936–2944. <https://doi.org/10.1016/j.bpj.2012.05.017>.
38. Sardo L, Hatch SC, Chen J, Nikolaitchik O, Burdick RC, Chen D, Westlake CJ, Lockett S, Pathak VK, Hu WS. 2015. Dynamics of HIV-1 RNA near the plasma membrane during virus assembly. *J Virol* 89:10832–10840. <https://doi.org/10.1128/JVI.01146-15>.
39. Chen J, Grunwald D, Sardo L, Galli A, Plisov S, Nikolaitchik OA, Chen D, Lockett S, Larson DR, Pathak VK, Hu W-S. 2014. Cytoplasmic HIV-1 RNA is mainly transported by diffusion in the presence or absence of Gag protein. *Proc Natl Acad Sci U S A* 111:E5205–E5213. <https://doi.org/10.1073/pnas.1413169111>.
40. Jouvenet N, Simon SM, Bieniasz PD. 2009. Imaging the interaction of HIV-1 genomes and Gag during assembly of individual viral particles. *Proc Natl Acad Sci U S A* 106:19114–19119. <https://doi.org/10.1073/pnas.0907364106>.
41. Chen J, Rahman SA, Nikolaitchik OA, Grunwald D, Sardo L, Burdick RC, Plisov S, Liang E, Tai S, Pathak VK, Hu WS. 2016. HIV-1 RNA genome dimerizes on the plasma membrane in the presence of Gag protein. *Proc Natl Acad Sci U S A* 113:E201–E208. <https://doi.org/10.1073/pnas.1518572113>.
42. Larson DR, Zenklusen D, Wu B, Chao JA, Singer RH. 2011. Real-time observation of transcription initiation and elongation on an endogenous yeast gene. *Science* 332:475–478. <https://doi.org/10.1126/science.1202142>.
43. Zenklusen D, Larson DR, Singer RH. 2008. Single-RNA counting reveals alternative modes of gene expression in yeast. *Nat Struct Mol Biol* 15:1263–1271. <https://doi.org/10.1038/nsmb.1514>.
44. Burdick RC, Delviks-Frankenberry KA, Chen J, Janaka SK, Sastri J, Hu WS, Pathak VK. 2017. Dynamics and regulation of nuclear import and nuclear movements of HIV-1 complexes. *PLoS Pathog* 13:e1006570. <https://doi.org/10.1371/journal.ppat.1006570>.